

Detailed mapping of metal deposit-related minerals by a combination of hyper- and multi-spectral images with geological information

Nguyen Tien Hoang* and Katsuaki Koike*

*Graduate School of Engineering, Kyoto University, Katsura C1-2-215, Kyoto 615-8540, Japan.

E-mail: koike.katsuaki.5x@kyoto-u.ac.jp (K. Koike)

Key words: Mineral mapping, AVIRIS, WorldView-3, Hydrothermal alteration, Cuprite

1. Introduction

Remote sensing has been effectively applied in geology with a low cost and minimal risk. Resource-related minerals on the Earth surface in sparsely vegetated areas can be detected and mapped from remotely sensed image by combining geological and structural mappings with the recognition of hydrothermally altered rocks. Generation of epithermal vein-type deposits has been mostly related to hydrothermal alteration of the adjacent country rocks (Sabins, 1999).

Multispectral and hyperspectral remote sensing have been widely used for mineral mapping and resource exploration (van der Meer *et al.*, 2012). Hyperspectral imagery has proven its capability for detailed discrimination of various types of Earth surface materials because of having hundreds of bands with high spectral resolution. Hyperspectral instruments have been increasingly developed including airborne sensors such as AVIRIS and HyMAP, and spaceborne sensors such as EO-1 Hyperion. Despite using a small number of bands, multispectral imagery with high spatial resolution is also effective in terms of signal to noise ratio and identifying mineral groups with small distribution areas (Hoang and Koike, 2018). Based on that background, this research is aimed to propose a new data combination of hyperspectral and multispectral remote sensing, geology, and field survey for improving the accuracy of mineral identification.

2. Data and study area

An integration of AVIRIS, a hyperspectral sensor covering the 0.4–2.5 μm range with 224 contiguous spectral bands, and WorldView-3, the first multi-payload and highest resolution commercial satellite sensor, was selected to test the accuracy of mineral mapping in the Cuprite area in the western United States (Fig. 1). An AVIRIS flight has to be requested months in advance and can cost upwards of 70,000 USD. Obtaining AVIRIS archived data from the years 2006 to 2018 is free of charge though the AVIRIS Data Products



Figure 1. Location of the Cuprite study area.

Portal. The pixel size of AVIRIS image is 15.7 m. WorldView-3 consists of eight visible-to-near infrared bands with 1.2-m spatial resolution, eight shortwave infrared (SWIR) bands with 7.5-m spatial resolution, and one panchromatic band with 0.31-m spatial resolution.

The study area consists of two main centers, which were formed by extensive development of the late-Miocene advanced argillic zones of iron-bearing minerals, clays, micas, sulfates, and carbonates. Because of the geological and surface conditions, which is mostly desert with sparse vegetation, Cuprite has been a suitable site to test the accuracy of mineral mapping through various remote sensing imagery produced by airborne and orbital visible, near-infrared, thermal-infrared, and hyperspectral sensors (Swayze *et al.*, 2014; Hoang and Koike, 2017).

AVIRIS and WorldView-3 scenes were acquired on 6 March 2013 and 19 September 2014, respectively. The field survey was carried out for four days from the end of October to the beginning of November in 2017. More than 100 rock samples were collected during this field survey as the ground truth data and then, their spectral reflectance were measured using FieldSpec 4 spectroradiometer and the mineral compositions were identified by X-ray diffraction. Preceding field survey data published by USGS were also referred in this study.

3. Methodology

As a main part of the data preparation step, atmospheric correction was applied to both the AVIRIS and WorldView-3 images. For this, both the images were atmospherically corrected using the Fast Line-of-sight Atmospheric Analysis of Spectral Hypercubes (FLAASH) module of ENVI software. Subsequently, the AVIRIS image was processed using the Spectral Hourglass Wizard package in ENVI software and following the step-by-step workflow of hyperspectral image-based mineral mapping in Kruse *et al.* (2003).

First, noises of reflectance band data were removed by Minimum Noise Fraction transformation, and computational requirements were reduced for the subsequent processing. Second, by repeatedly projecting n-D scatter plots on a random unit vector, the Pixel Purity Index was computed from the MNF output to collect the most spectrally pure pixels in the image. Third, n-dimensional visualization of large PPI value pixels was performed to locate and group the purest pixels into classes. Mineral endmembers were then identified by comparing spectral profiles of the purest pixels with the USGS spectral library and considering ground truth data measurements. Finally, the distribution and abundance

of selected minerals were mapped by the mixture-tuned matched filtering (MTMF) method integrated with several mineral indices, such as hydroxyl, Al-OH-bearing, Mg-OH-bearing, Fe-OH-bearing, iron-stained, carbonate, kaolinite, calcite, and jarosite indices, which were calculated from the WorldView-3 image.

4. Results and discussion

The MTMF of AVIRIS image provided a set of two-rule images, showing the MF score and infeasibility value at each pixel by comparing the spectrum of each endmember. Through this procedure, a mineral map of the distribution and abundance of a selected mineral was produced. Based on the scatter-plot trend between the MF score and infeasibility value, a selected mineral was assigned to each pixel with small infeasibility value and large MF score in which 1.0 is the perfect match. Subsequently, the optimal threshold was selected on a case-by-case basis to represent well the results of WorldView-3-based mineral indices calculation and field survey data. At a pixel in which multiple endmembers were mixed, the endmember with the largest MF score was selected as the representative mineral there.

In total, more than ten mineral categories were mapped and verified by the laboratory analyses of field samples. These categories include iron-bearing minerals, clays, micas, sulfates, and carbonates. Figure 2 compares spectral profiles of K-alunite by the AVIRIS and WorldView-3 images, the USGS library, and the FieldSpec 4 spectrometer of a sample, and shows an XRD chart representing conspicuous presence of K-alunite. The main absorptions of K-alunite in SWIR region clearly appear in the AVIRIS spectral profile but not in the WorldView-3 profile. The reflectance absorptions of jarosite, goethite, and hematite in the electronic region (0.4–1.3 μm) were successfully differentiated within the study area. In addition, the distribution of minerals with absorption features in the vibrational region (1.3–2.5 μm) provides the most detailed map of advanced argillic alteration. Consequently, the resultant map clarifies the complex distributions of minerals in Cuprite, including homogeneous and heterogeneous zones of mineral composition (Fig. 3).

5. Conclusion

Hyperspectral remote sensing, in conjunction with multispectral remote sensing, geology, and field survey, allowed the detailed mapping of hydrothermal alteration zones in the Cuprite area. The application of AVIRIS image and multiple data integration method are expected to improve the accuracy of mineral exploration. An additional analysis is necessary to distinguish opal and chalcedony in the hydrated silica zones.

References

Hoang, N. T., & Koike, K. (2017) Transformation of Landsat imagery into pseudo-hyperspectral imagery by a multiple regression-based model with application to metal deposit-related minerals mapping. *ISPRS-J. Photogramm. Remote Sens.*, vol.133, pp. 157-173.
 Hoang, N. T., & Koike, K. (2018) Comparison of hyperspectral transformation accuracies of multispectral Landsat TM, ETM+, OLI and EO-1 ALI images for detecting minerals in a geothermal prospect area. *ISPRS-J. Photogramm. Remote Sens.*, vol.137, pp. 15-28.
 Kruse, F. A., Boardman, J. W., & Huntington, J. F. (2003)

Comparison of airborne hyperspectral data and EO-1 Hyperion for mineral mapping. *IEEE Trans. Geosci. Remote Sensing*, vol.41, pp. 1388-1400.
 van der Meer, F. D. *et al.* (2012) Multi- and hyperspectral geologic remote sensing: A review. *Int. J. Appl. Earth Obs. Geoinf.*, vol.14, pp. 112–128.
 Sabins, F. F. (1999) Remote sensing for mineral exploration. *Ore Geol. Rev.*, vol.14, pp. 157–183.
 Swayze, G. A. *et al.* (2014) Mapping advanced argillic alteration at cuprite, Nevada, using imaging spectroscopy. *Econ. Geol.*, vol.109, pp. 1179–1221.

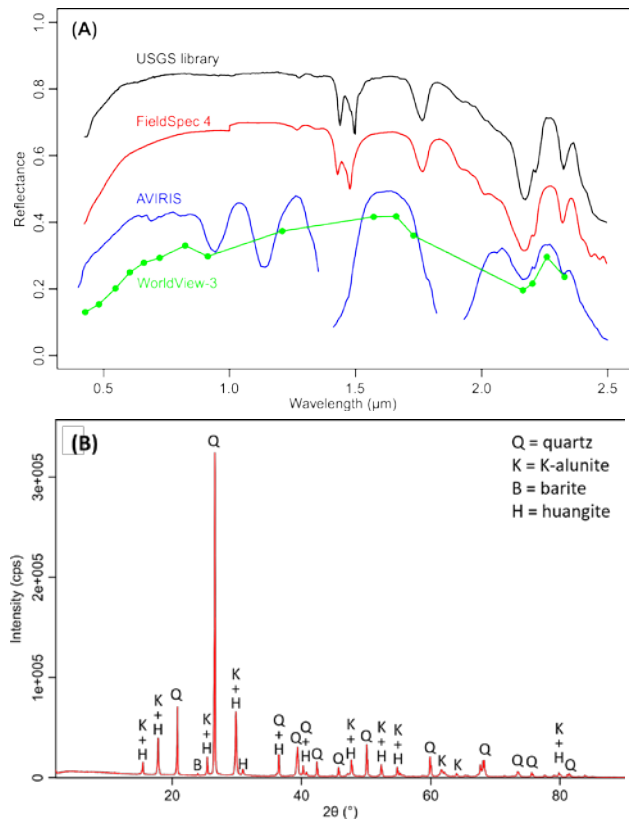


Figure 2. (A) Comparison of spectral profiles of K-alunite by the AVIRIS and WorldView-3 images, the USGS library, and the FieldSpec 4 spectroradiometer of a sample. (B) XRD chart of a sample showing conspicuous presence of K-alunite. Each profile of the AVIRIS and WorldView-3 images is spectral curve of a pixel covering the sampling location.

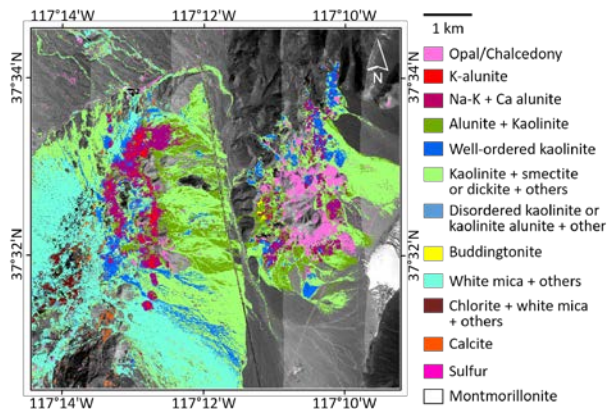


Figure 3. MTMF mineral maps showing the most dominant endmember in each pixel, produced from the AVIRIS image.